M₂ BAROCLINIC TIDES in the Indonesian Seas

BY ROBIN ROBERTSON AND AMY FFIELD

Baroclinic, or internal, tides play a significant role in mixing in the deep ocean and in shallow seas (Munk and Wunsch, 1998; Garrett, 2003). In a stratified ocean, when the vertically uniform horizontal velocities of barotropic tides (tides in which surfaces of constant pressure are parallel to surfaces of constant density) interact with rough topography, disturbing isotherms and isopycnals, they generate baroclinic tides, for which the velocities are not vertically uniform. Currents, internal waves, and heaving isotherms resulting from baroclinic tides affect forces on structures and vessels. Vigorous internal tides have been observed in the Indonesian seas with isotherm excursions up to 90 m in the Ceram Sea during 14-hour yo-yo stations (Ffield and Gordon, 1996). Tides also affect the generation of mean currents and mixing. Mixing processes modify the ocean's hydrography, or physical characteristics, leading to density-driven flows. In the Indonesian seas, mixing transforms the Pacific inflow waters into Indonesian throughflow waters (Gordon, this issue) before export to the Indian Ocean. We used a tidal model to simulate the barotropic and baroclinic tides in the Indonesian seas to verify model performance against observations and to provide examples of baroclinic tidal activity.

Although internal tides have been observed in the Indonesian seas, the baroclinic tidal fields are not well known. In particular, relatively few full-depth, long-period current observations suitable for accurately quantifying the baroclinic tidal fields exist. More complete coverage has been provided by modeling studies; good replication of the barotropic fields has been obtained by Mazzega and Bergé (1994), Hatayama et al. (1996), and Egbert and Erofeeva (2002) using two-dimensional simulations. For the baroclinic tides, three-dimensional simulation is required to include vertical variability. Schiller (2004) and Simmons et al. (2004) simulated the baroclinic tides in the Indonesian seas on coarse grids (~0.5° in latitude and longitude, or ~50 km) using a z-level model (Modular Ocean Model [MOM]) and an isopycnal model, respectively. However, the grid cell sizes of these simulations are inadequate to resolve the internal tides

in depths less than 2000 m where the internal tidal wavelength ranges from ~20–50 km. Grid cells of 4–5 km or finer are required to resolve the internal wavelengths in shallow water (Holloway, 2001). In a study for Fieberling Guyot (Robertson, submitted), a resolution of 1 km was required to accurately predict mean currents and major axis amplitudes. In the Fieberling Guyot study, model performance improved with higher-resolution (< 1 km) bathymetry and more vertical layers; however, a resolution of ~5 km was sufficient for indicating where baroclinic tides occur.

In this study, our goal is to estimate the baroclinic tidal fields for the Indonesian seas to provide baroclinic tidal information for future observational programs and focused regional modeling studies. Computing limitations require a balance between geographic coverage and model performance, which is resolution dependent. For our overview, we selected a resolution of 5 km in order to include the entire Indonesian seas region, realizing that this would be a more qualitative estimate than an accurate quantitative estimate.

...our goal is to estimate the baroclinic tidal fields for the Indonesian seas to provide baroclinic tidal information for future observational programs and focused regional modeling studies.

TIDALLY INDUCED EFFECTS

Interactions of the tides with bottom topography affect circulation and mixing, both as mean and oscillating effects. Our focus is the latter. In a stratified ocean, internal waves can be generated when the tide interacts with topography and the tidal frequency [ω] falls between the inertial frequency [f] and the buoyancy frequency [N] (i.e., equatorward of the critical latitude). The critical latitude is defined as the location where the inertial frequency equals the tidal frequency: 28–30° latitude for the diurnal constituents and 74.5–86° latitude for the semidiurnals. According to linear internal wave theory, the strength of internal-wave generation is dependent on the stratification characterized by the buoyancy frequency, the inertial frequency, and the steepness of the bathymetry with the strongest generation, both in amount and magnitude, occurring when the steepness of the bathymetry is roughly equivalent to the slope of the internal wave characteristics:

$$\sqrt{\frac{\omega^2 - f^2}{N^2 - \omega^2}}$$

In the Indonesian seas, this criterion predicts internal tides generation by steep topography at both diurnal and semidiurnal frequencies over much of the domain.

TIDAL MODEL

We simulated tides using a primitive-equation, terrain-following coordinate model, the Regional Ocean Model System (ROMS) (http://marine.rutgers.edu/po/index.php?model=roms). This model has been used for simulating tides for various regions (Robertson et al., 2003; Robertson, 2005a, 2005b). The domain (yellow box in Figure 1a) covers much of the Indonesian Seas with a horizontal resolution of 5 km (Figure 1b) and 24 vertical levels. Realistic bathymetry was taken from Smith and Sandwell (1997) using the 0 m isobath as the coastline; water depths shallower than 50 m were deepened to 50 m. Smoothing was applied using repeated Gaussian weighting in areas that exceeded the steepness tolerance of the model. Hydrographic fields, potential temperature, and salinity for the domain were optimally interpolated from observational profiles in the region obtained from the National Oceanographic Data Center. Tidal forcing focused on a single constituent, the M_2 tide with a period of 12.42 hrs, and was implemented by prescribing the M_2 elevations along the open boundaries using TPXO6.2 results (Egbert and Erofeeva, 2002). Flather radiative boundary conditions were used for the normal 2-D velocities, advective conditions for the 2-D tangential velocities, Martinsen and Engedahl (1987) flow relaxation over four cells for the 3-D velocities, and relaxation over four cells for the tracers. There were no surface or bottom fluxes of tracers and the volume was unconstrained. A fuller description of the model, boundary conditions, and forcing can be found in Robertson et al. (2003). The model was run for five days before data were saved for analysis, which was sufficient for the energies to stabilize. The small portion of the Sulu Sea that is included in the domain and much of the region adjacent to the boundaries will be ignored, due to the influence of model boundary effects.

TIDAL OBSERVATIONS

Model performance evaluation requires observations of both elevation (i.e., sea level) and velocities at multiple depths. Thirteen *TOPEX/Poseidon* (T/P) satellite crossover observations of elevations (yellow crosses in Figure 1a and Table 1)

For more accurate quantitative estimates, higher horizontal and vertical resolutions are required.

and four moorings with velocities observations at multiple depths (red stars in Figure 1) were used. The T/P crossover points of elevation observations were provided as amplitudes and phase lags from the PATHFINDER data base (contact R. Ray, rray@geodesy2.gsfc.nasa.gov). Current-meter mooring data from the two Makassar moorings were analyzed for tides using the *T_Tide* software (Pawlowicz et al., 2002), which also provided estimates of the observational uncertainty.

ELEVATIONS

Model estimates of the M_2 tidal elevation amplitudes range from 20–50 cm

Robin Robertson (*rroberts@ldeo.columbia.edu*) *is Doherty Associate Research Scientist, Lamont-Doherty Earth Observatory, Palisades, NY, USA.* **Amy Ffield** *is Senior Scientist, Earth & Space Research, Upper Grandview, NY, USA.*
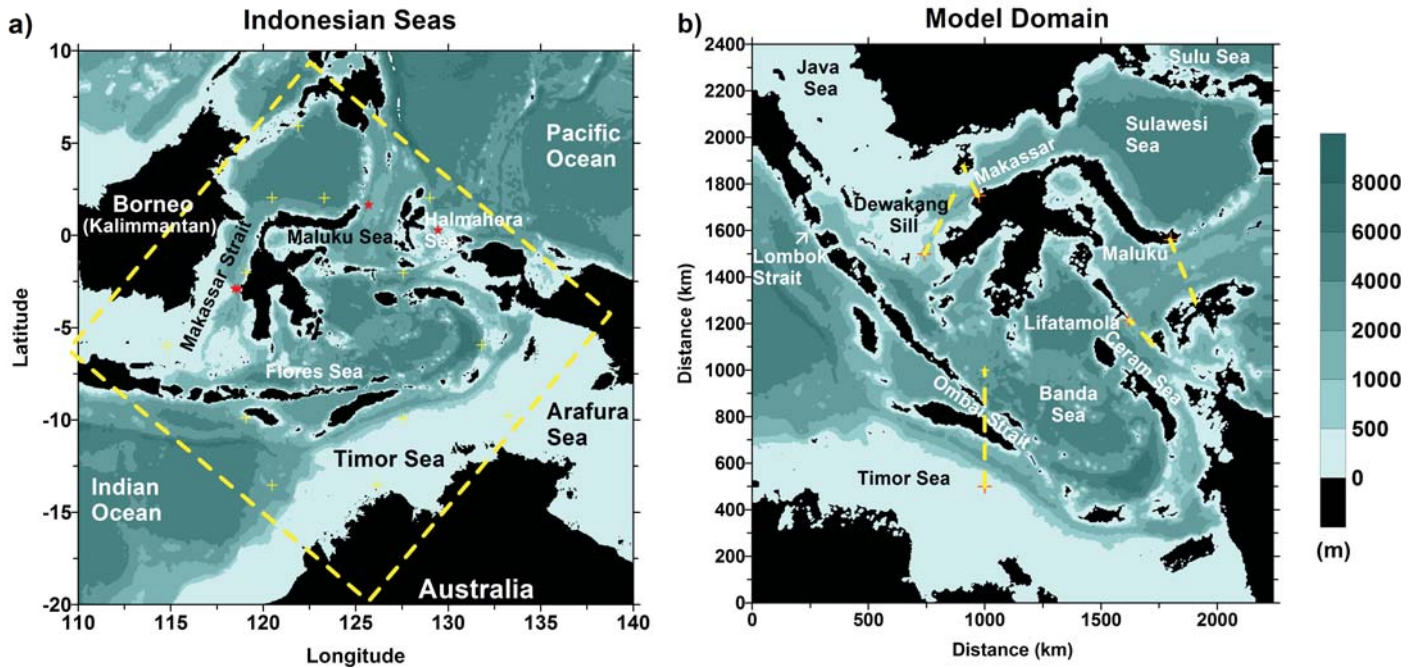
Figure 1. (a) The bathymetry of the Indonesian Seas with some of the major features identified. The model domain is indicated by a yellow dashed box and the locations of *TOPEX/Poseidon* crossover elevation observations by yellow crosses. Current meter mooring locations in the Makassar Strait and Maluku and Halmahera Seas are marked with red stars. (b) The bathymetry over the model domain. Transect locations of Figure 4 are indicated by yellow dashed lines with a red cross at the origin.

Table 1. M_2 elevation amplitude and phase lags comparison between T/P crossover observations and model estimates at the locations shown as yellow crosses in Figure 1a. The differences and rms of the differences are given for both the amplitudes and phase lags.

| Site	Latitude	Longitude	M_2					
			Amplitude (cm)			Phase Lag (o)		
			Obs.	ROMS	Diff.	Obs.	ROMS	Diff.
1	5° 56' N	121° 53'E	59.6	66	+6	290	298	+8
2	2° 9' N	120° 28'E	58.9	71	+12	290	300	+10
3	2° 2' N	123°17' E	57.2	65	+8	291	297	+6
4	2° 1' N	128°58' E	49.3	46	-3	288	279	-9
5	2° 3' S	127° 33'E	25.6	21	-5	160	165	+5
6	2° 9' S	119° 3' E	46.4	46	0	277	298	+21
7	5° 54' S	131° 49'E	58.5	51	-8	139	154	+15
8	5° 58' S	114° 48'E	13.4	19	+6	140	126	-14
9	9° 45' S	127° 33' E	62.2	51	-11	120	125	+5
10	9° 45' S	119° 3' E	83.1	91	+8	54	66	+12
11	9° 46' S	133° 13'E	43.5	101	+57	189	189	0
12	13° 30'S	126° 8'E	84.7	68	-15	62	34	-28
13	13° 31'S	120° 28'E	89.7	94	+4	56	66	+10
Rms differences: all sites			18			13		
Rms differences: excluding site 11			8			13		
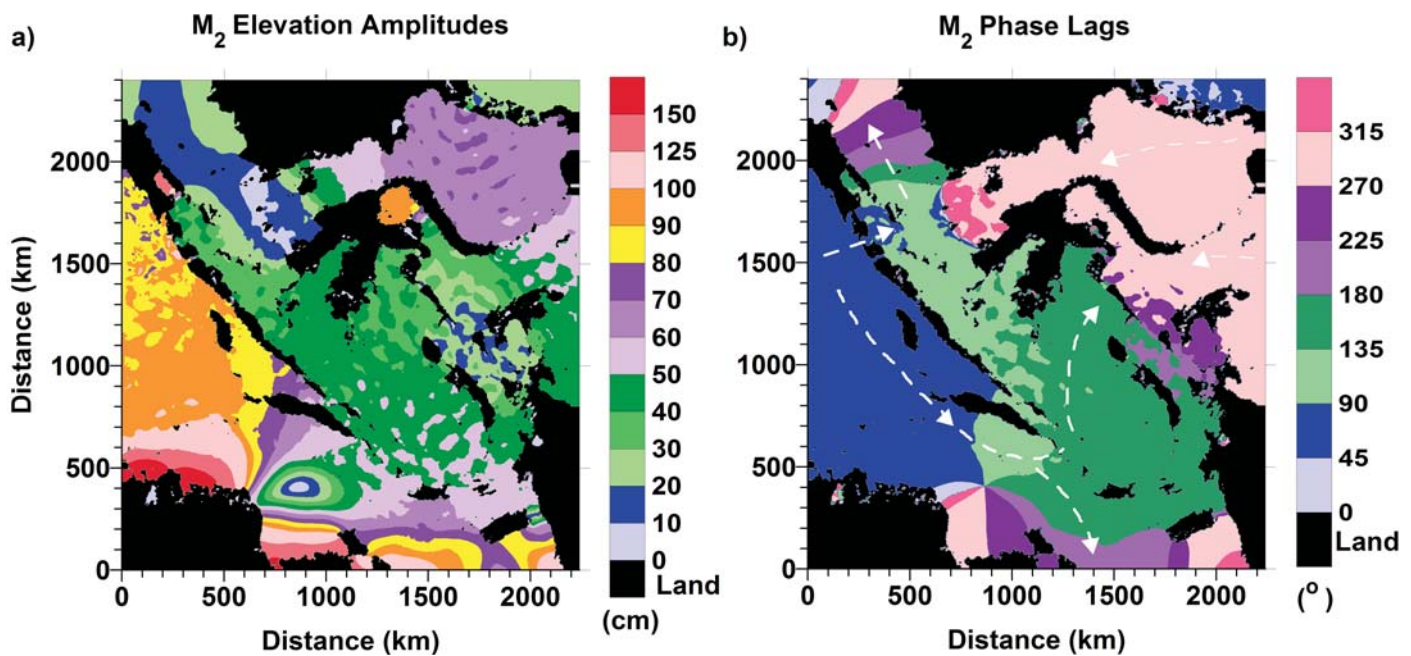
Figure 2. (a) The elevation amplitude for the M$_2$ tidal constituent over the model domain. M$_2$ elevations amplitudes ranged from 20–50 cm over most of the domain, with higher amplitudes reached in the Indian Ocean, Sulawesi Sea, and along the Australian coast. Lower amplitudes occurred in the Java and Ceram Seas. (b) The phase lag for the M$_2$ elevation over the model domain with the direction of propagation indicated by white arrows. The tide propagates from the Indian Ocean through the Timor Sea, where an amphidromic point forms. A portion of the tide also propagates from the Indian Ocean through Lombok Strait into the region south of Makassar Strait. In the Timor Sea, the tide splits with a portion going into the Arafura Sea and another into the Banda Seas. In the Banda Sea, the tide splits again with a portion going into the Flores Sea and another north into the Ceram Sea. South of Makassar Strait is a confluence region for the portions from Lombok Strait, the Flores Sea, and the weaker portion from the Pacific Ocean (thinner arrows) via Makassar Strait. From there, it exits via the Java Sea.

through most of the region (Figure 2a). Higher amplitudes occur in the Sulawesi Sea, Indian Ocean, and shallow regions, including along the Australian coast where they exceed 150 cm. Lower amplitudes, < 20 cm, occur in the Java and Ceram Seas, and near an amphidromic point (low-amplitude point with phase changing rapidly through 360°), which forms in the Timor Sea.

The M$_2$ tide enters this region of the Indonesian seas both from the Indian Ocean and the Pacific, with stronger tides from the Indian Ocean. As evidenced by the phase lag (Figure 2b), the M$_2$ tide progresses from the Indian Ocean through the Timor Sea, where an amphidromic point forms. Additionally,

a portion passes through Lombok Strait into the region south of Makassar Strait. In the Timor Sea, it splits with one portion progressing into the Banda Sea and another into the Arafura Sea. The speed, c, of tidal progression is dependent on the water depth, H, ($c = \sqrt{gH}$, where g is gravity, 9.8 m s^{-2}). The tide progresses rapidly in the deep Banda Sea (with bottom depths exceeding 7000 m in the Weber Basin), resulting in little change in phase lag. In the Banda Sea, the tide continues into the Ceram Sea, which is a confluence region, where the Indian Ocean tide meets that of the Pacific, resulting in a reduction of the tidal amplitudes. Another confluence region occurs at the southern end of Makassar Strait,

where the tide coming through Lombok Strait meets the Pacific tide coming through Makassar Strait. The tide exits this region through the Java Sea. In the Java Sea, the water depth is very shallow, less than 70 m, and the tide progresses slowly, resulting in closely spaced phase lag lines (Figure 2b).

These estimates reasonably match the 2-D inverse simulations of Mazzega and Bergé (1994) and Egbert and Erofeeva (2002), and the 2-D simulations of Hatayama et al. (1996) and Ray et al. (this issue). Our 3-D simulation, which is not an inverse model, reasonably reproduces the elevations when compared to the T/P satellite crossover elevation observations (yellow crosses in Figure 1a). Differences

between the T/P observations and the model estimates are generally small (< 10 cm and <15°) (Table 1). Phase-lag differences > 20° occur in areas of rapidly changing phase (near the amphidromic point in the Timor Sea and in Makassar Strait), where small differences in location or bathymetry result in large phase differences. Rms differences between T/P crossover observations and the model estimates were 18 cm for the amplitude and 13° for the phase lag with all 13 sites included. The largest discrepancy (+57 cm) occurs at Site 11, which is both in shallow water and near the boundary. This site is within a few kilometers of very shallow water (28 m), which can be problematic for both T/P analysis and the model estimates. Removing Site 11 reduces the rms values to 8 cm and 13°. These discrepancies may be associated with inaccuracies in the bathymetry and the hydrography because neither is well known.

VELOCITIES

The model provides two velocity fields: a depth-independent or barotropic velocity field and a depth-dependent velocity field. Both are complete estimates of the velocity fields (i.e., the depth-independent velocity does NOT need to be added to the depth-dependent velocity). The depth-dependent velocities include the barotropic or depth-independent motion through the barotropic-baroclinic mode linkage in the model. Tidal currents are described using a tidal ellipse, which is traced by the tip of the current vector during one complete cycle. The tidal ellipse is specified by the major and minor axes representing the maximum and minimum tidal currents along with the inclination of the orbits and the phase (Figure 3a). Discussion of ma-

jor axes reflects only the portion of the maximum velocities at the frequency of the tidal constituent, here M_2. However, the velocity fields contain contributions at other frequencies and at the mean and are comprised of geostrophic velocities, tidal residual velocities, harmonic responses, and tidal mixing-induced density-driven velocities, along with the barotropic and baroclinic tides and various other oscillations.

The barotropic or depth-independent M_2 major axes are small (< 2 cm s^{-1}) over much of the region (Figure 3b) with higher velocities in shallow water. High major axes occurred in straits, where the fluid is forced through the narrow channels, occasionally reaching major axes of over 50 cm s^{-1}. The magnitude of the barotropic major axes correlates with the topography, with low major axes in deep water and high values in shallow water and narrow straits.

The M_2 major axes are strongly depth-dependent particularly in straits and near rough topography, indicating the generation and propagation of internal tides. This is clearly seen in a selection of transects of the major axes (Figure 4), with their locations indicated in Figure 1b. Beams of large major axes radiate from sills and ridges propagating towards the surface (Figure 4b–e). Large baroclinic major axes occur in the Maluku Sea and Ombai, Lifamatola, and Makassar Straits (Figure 4a–c), which also have large barotropic tides (Figure 3a). The transects in Figure 4 show various baroclinic responses according to their conditions.

The Lifamatola Strait transect (Figure 1b) lies between the Maluku and Ceram Seas where the barotropic tide propagating from the Indian and Pacific Oceans

meet, reducing the tidal elevations (Figure 2a). In contrast to the elevations, both the barotropic (Figure 3b) and the baroclinic (Figure 4a) M_2 tidal velocities are high. A strong benthic baroclinic tide occurs on the western side and two baroclinic tidal beams originate from the eastern slope at 500 and 800 m water depth.

Along the transect in the Timor Sea and across Ombai Strait into the Banda Sea (Figure 1b), baroclinic tides are generated primarily in three locations: over the Australian slope, on the southern shoulder of Timor Island propagating offshore, and over the sill north of the Ombai Strait propagating both into the strait and northwest into the Banda Sea (Figure 4b). The strongest internal tides occur in the Ombai Strait, with major axes > 50 cm s^{-1}. Focusing on the Ombai Strait because it is a clear example, baroclinic tides are evident in the temperature fields, with isotherm fluctuations of 50–200 m (Figure 5a–c). These fluctuations propagate away from the sill into the strait in the three snapshots, which are 6 hrs apart (~M_2 tidal cycle). The horizontal and vertical model resolutions are barely adequate to resolve these waves. But, isotherm depths and temperature-layer thicknesses are clearly modified with time as the internal tides propagate.

In the transect along the Maluku Sea (Figure 4c), internal tides generated over rough topography propagate into the upper water column where the internal wave rays become more horizontal due to stronger stratification. The major axes increase in the strongly stratified layer. In the eastern basin, much of the response appears not to be locally generated, but generated nearby, propagating into the transect. This includes the surface response generated along the coast.

The transect through the restriction in Makassar Strait (Figure 1b) shows a strong baroclinic tide originating at the western shoulder and propagating across the strait and a bottom-trapped tide at the eastern edge (Figure 4d). These peaks may not be generated by topographic features along the transect, but by off-transect features with propagation into the transect.

In the transect over Dewakang Sill at the southern end of Makassar Strait (Figure 1b), undulations of the sill generate baroclinic tides both over the northern hump and at the trough between the
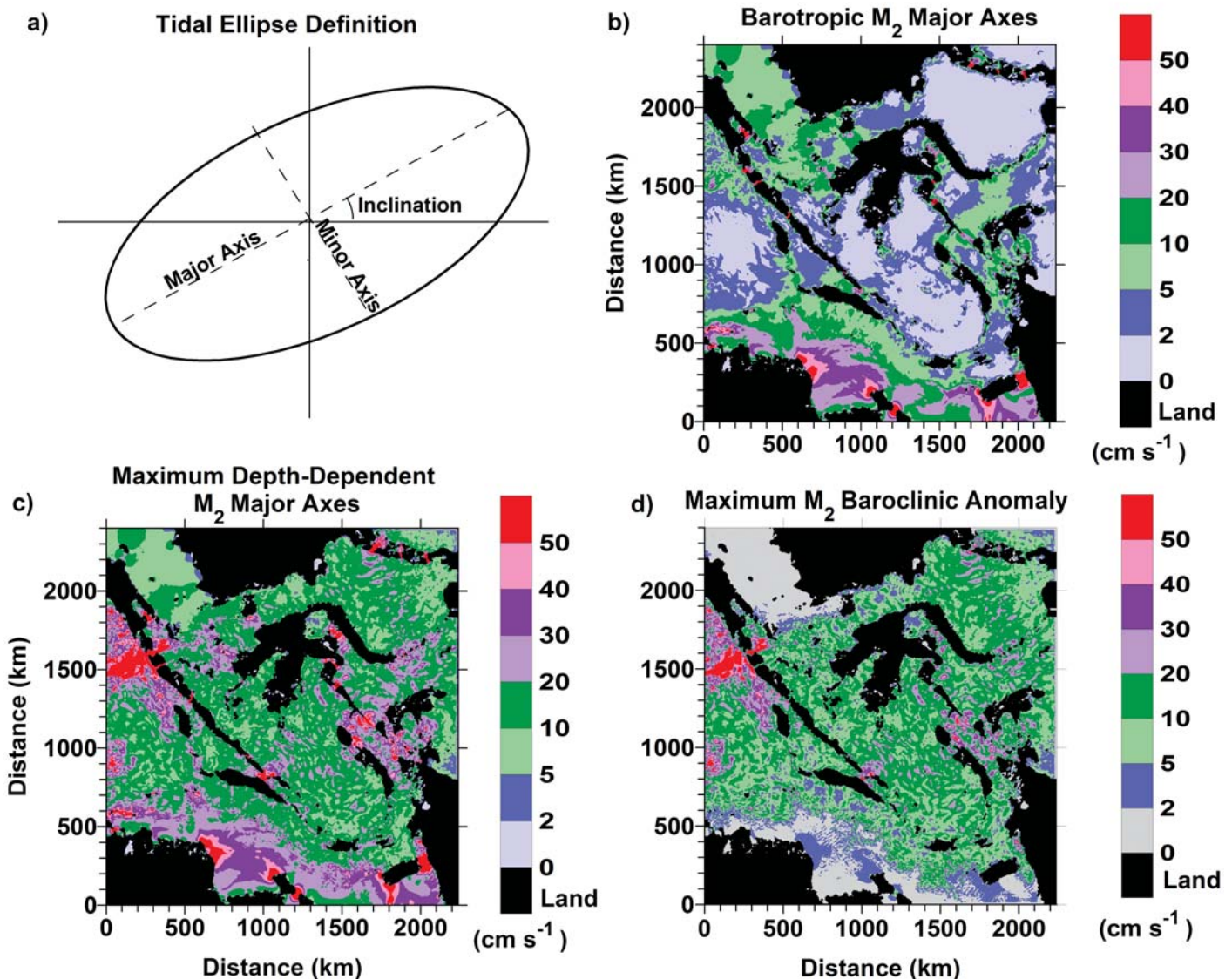

Figure 3. (a) A tidal ellipse is defined by the major axis, the minor axis, and the inclination. A phase (not shown) is also used for replicating currents. (b) Amplitudes of the major axis of the M_2 tidal ellipses from the depth-independent velocity. The major axes are small in the deep basin areas and large in the shallow Java, Timor and Arafura Seas. The largest barotropic major axes, > 50 cm s^{-1}, occur in narrow straits. (c) The maximum depth-dependent major axes in the water column at each grid cell of the M_2 tidal ellipses are higher than the depth-independent or barotropic major axes over much of the domain, including the Sulawesi, Ceram, and Banda Seas and the Makassar Strait. (d) The maximum baroclinic anomaly for M_2, with the baroclinic anomaly defined as the difference between the depth-independent and maximum depth-dependent major axes. The highest maximum baroclinic anomalies occur in the Sulawesi and Ceram Seas, in Ombai Strait, and south of Lombok Strait.

humps. These tides propagate in both directions (Figure 4e). Even small fluctuations of the bathymetry generate internal tides here although some of the high values are attributable to off-transect generation. This region is noted for high baroclinic tides and mixing, with the tidal field highly sensitive to the topographic undulations (Hatayama, 2004). Lee waves were generated in Hatayama's non-hydrostatic model, but our simulation does not include these lee waves or internal solitons, because it is hydrostatic.

To evaluate the model performance in replicating baroclinic tides, model estimates were compared to velocity observations from moorings with multiple instruments. For logistical reasons, these observations are difficult to obtain due to strong oscillating currents, fouling from high biological productivity, and high ship traffic in the regions, particularly fishing net operations. A persistent problem is strong tidal currents pushing the mooring downwards, with the shallower meters easily pushed as much as 200 to 300 m deeper at some locations during the peak of each tidal cycle (Susanto and Gordon, 2005; Molcard et al., 2001). In fact, estimation of the M_2 barotropic, depth-independent, tidal currents are not attempted here, because none of the offshore current observations have
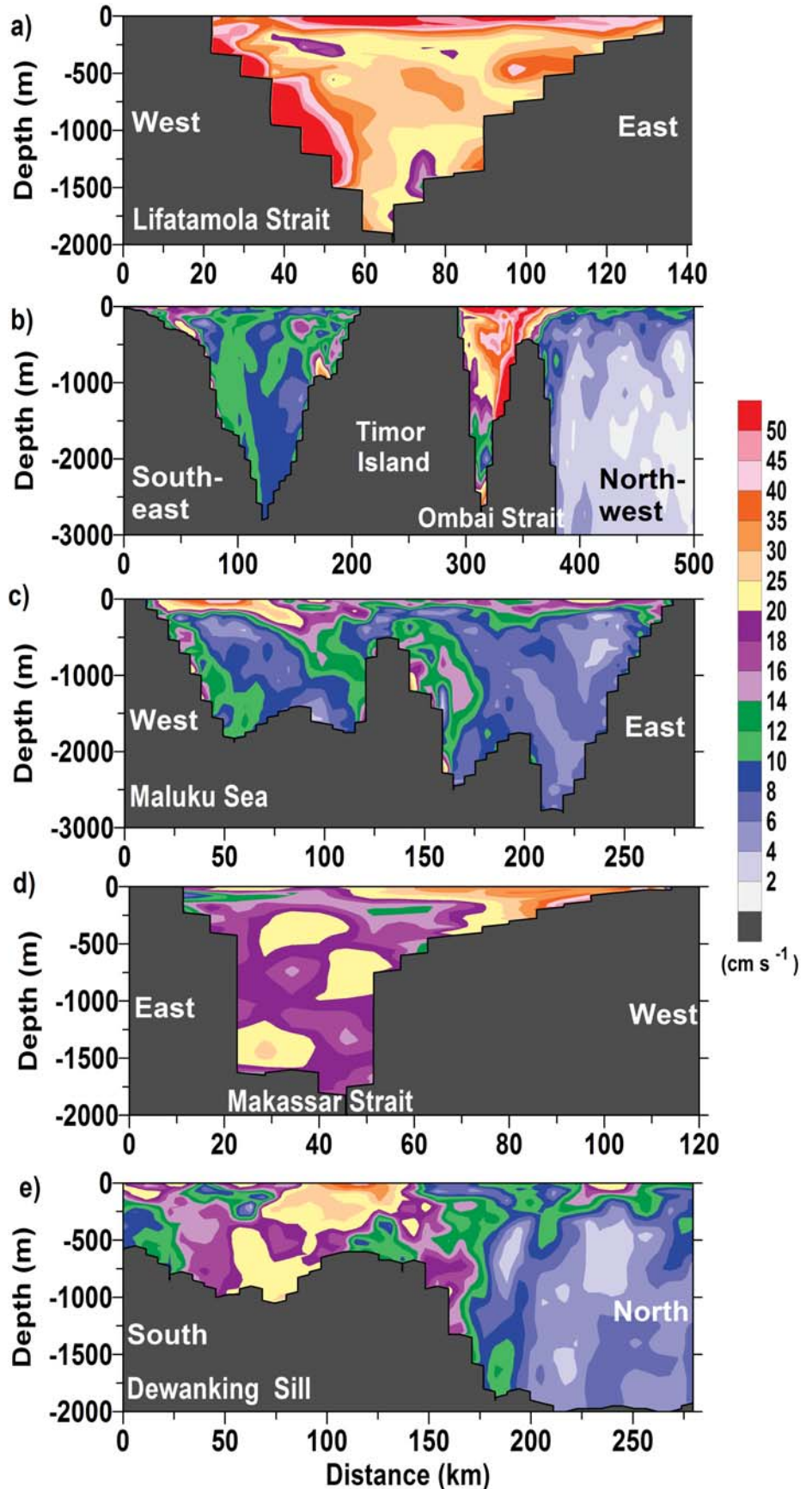

Figure 4. Transects of the major axes of the M_2 tidal ellipses from the depth-dependent velocity for the (a) Lifamatola Strait, (b) Timor and Ombai Straits, (c) Maluku Strait, (d) Makassar Strait, and (e) over Dewakang Sill. Large baroclinic responses occur in all transects, although some of the baroclinic responses were generated nearby, propagating into the transects.
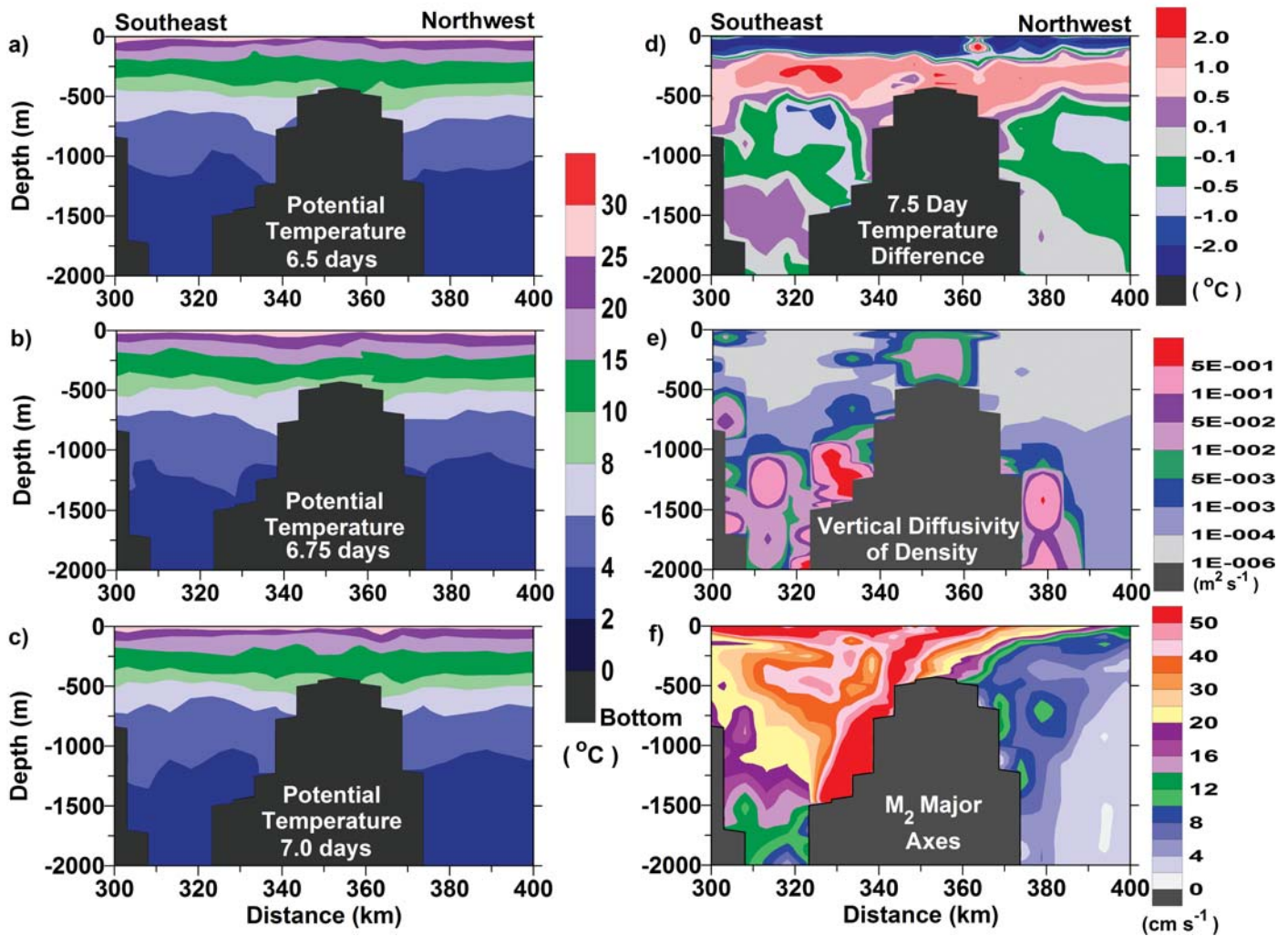
Figure 5. The temperature for a section of the Ombai Strait transect is shown at (a) 6.5 days, (b) 6.75 days, and (c) 7.0 days. The (d) 7.5 day temperature differences, (e) vertical diffusivity for temperature estimate, K_T, averaged over one day, and f) major axes of the M_2 tidal ellipses for the same section of the Ombai Strait transect. The isotherms and temperature layer thicknesses fluctuate with the tide in panels (a)–(c) with the isotherms fluctuating ~50–200 m. High vertical diffusivities over the sill and along the left flank in panel (e) coincide with the large gradient in the major axes f). Additionally, the high vertical diffusivity over the sill (e) coincides with the large 7.5 day temperature differences in panel (d). It is believed that these differences result from mixing over the sill and advection of the mixed fluid away from the sill in both directions.

sufficient depth and time resolution to attain an unbiased depth-average. The current-meter mooring records used here (red stars in Figure 1a) were readily available with published depth-dependent velocity statistical information, consisting of two moorings in Makassar Strait (Susanto and Gordon, 2005), which are < 20 km (four grid cells) apart

plus one in the Maluku Sea (Luick and Cresswell, 2001) and one in the Halmahera Sea (Cresswell and Luick, 2001). Unfortunately, all of these moorings were blown over by strong tidal currents. The uppermost current meter on the western Makassar mooring (1), was near its target depth of 200 m for only 6% of the record, whereas the uppermost

meter on the eastern Makassar mooring (2) was near its target depth of 205 m for 32% of the record and the next lower current meter on that mooring was near its target depth of 255 m for 85% of the record (Susanto and Gordon, 2005). Consequently, the eastern Makassar mooring 2 is assumed to be more accurate, particularly for the deeper estimates

where mooring blowover is reduced.

Comparison of the model estimates for the M_2 major axes to the observed values at the moorings are inconclusive (Figure 6). Although the Makassar mooring observations are similar to the model estimates (Figure 6a–b), with smaller differences for the more accurate mooring 2, the observations are insufficient to verify the patterns seen with the model. The model overestimates the velocities with the differences exceeding the observational uncertainty as determined by *T_Tide* (red error bars in Figure 6a–b). Blowover at the moorings resulted in a reduction of the major axes in the upper ocean for the observations where the model indicates an increase. The higher accuracy of the Makassar mooring 2 is reflected in a lower rms

difference between the observations and model estimates of 4.8 cm s⁻¹ for mooring 2, compared to 5.3 cm s⁻¹ for mooring 1. For the Maluku and Halmahera mooring, rms differences were 2.0 cm s⁻¹ and 3.0 cm s⁻¹, respectively. Both observational and model errors contribute to the discrepancies along with other factors such as water-depth differences between the model and the observations. At the mooring locations, differences in the observed water depths and the model depth range from ~200–400 m.

DISCUSSION: IMPLICATIONS OF THE TIDAL VELOCITIES

As discussed earlier, M_2 baroclinic tides occur throughout the region. The maximum depth-dependent M_2 major axes in the water column at each grid cell (Fig-

ure 3c) are significantly larger than the depth-independent or barotropic M_2 major axes (Figure 3b) over much of the region. They are of similar magnitude only in shallow water. To isolate the baroclinic M_2 major axes, the depth-independent M_2 major axes were removed from the maximum depth-dependent M_2 major axes without consideration of phase lag to determine the maximum M_2 baroclinic anomaly. The maximum M_2 baroclinic anomaly (Figure 3d) shows strong M_2 baroclinic tides (> 20 cm s⁻¹) over rough topography in the Sulawesi and Ceram Seas and many of the narrow straits. The maximum M_2 baroclinic anomaly is only low (< 2 cm s⁻¹) in the Java, Timor, and Arafura Seas.

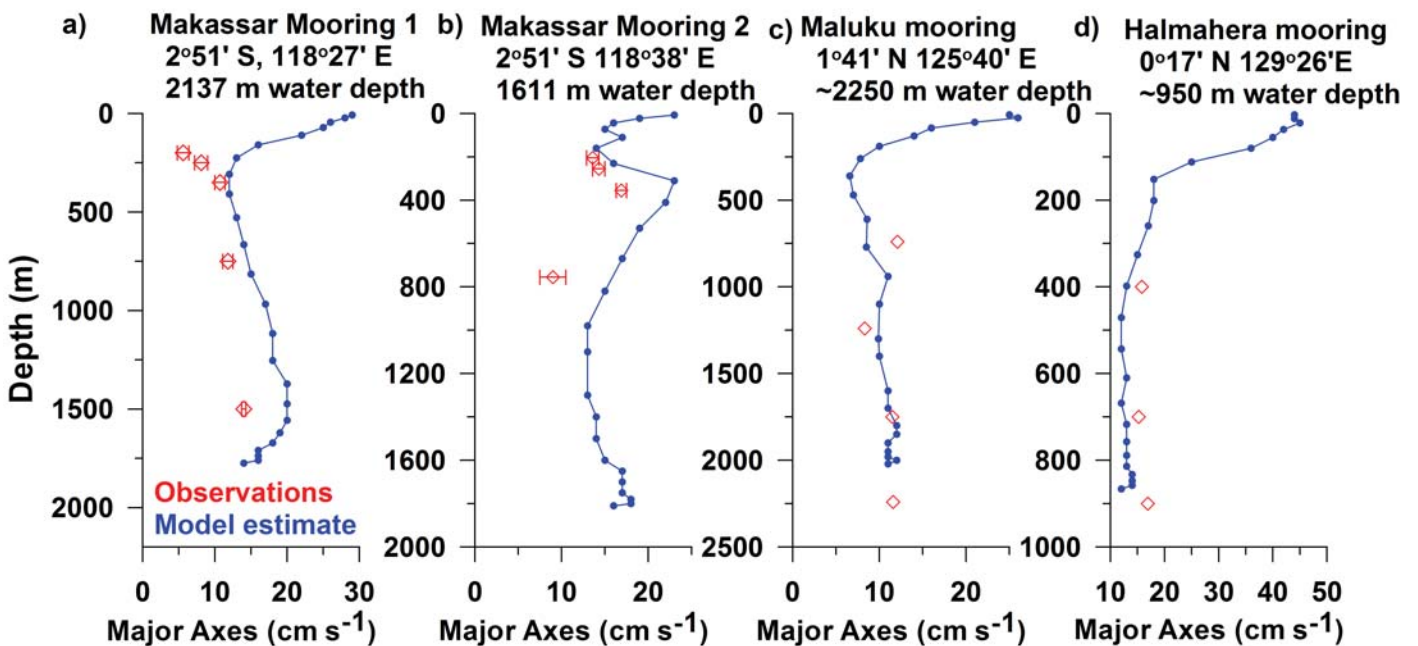Baroclinic tides induce vertical mixing, which is characterized by the vertical

Figure 6. The M_2 major axes at the Makassar Strait moorings (a) 1 and (b) 2, (c) the Maluku mooring and (d) the Halmahera mooring are indicated by a blue line with dots at the levels for the model estimates and red diamonds for the observations. The observational uncertainties as determined by *T_Tide* are indicated by error bars, when available.

mixing coefficient for density, K. Because in this application vertical diffusivities for temperature, K_T, and salinity, K_S, are the same, K_T is equivalent to K. K_T is calculated in the model according to the stratification and the vertical shear of the horizontal velocities using the dissipa-

500 m, reflecting an upper ocean heat transfer. The surface cooling is a result of lack of a surface radiative heat flux representing incoming solar radiation. This application also ignores freshwater fluxes representing net evaporation/precipitation. Mixing over the sill and along the

entire domain. The maximum baroclinic tidal anomalies, defined as the difference between the maximum depth-dependent major axes within the water column and the depth-independent major axes for each grid cell, were > 5 cm s^{-1} through most of the domain and > 20 cm s^{-1} over rough topography in the Sulawesi and Ceram Seas and in many of the straits. These tides induced modifications of the thickness of the density layers and isotherm displacements of 50 m near the thermocline. Larger isotherm displacements, reaching 200 m, occurred in the weaker stratification below the permanent pycnocline. High vertical mixing coefficients and large temperature differences often accompanied the baroclinic tides, occurring in the high shear zone adjacent to the internal tide beams.

Improved performance can also be obtained through more accurate bathymetry and hydrography.

tion-based version of the Generic Length Scale method. This method is based on the gradient Richardson number, Ri_g, which is a ratio of the stability of the water column to the vertical shear in the water column. An example of the model estimate for K_T averaged over one day for the Ombai Strait is shown in Figure 5e. Model estimates of K_T increase in the shear zone below the internal tide beams in the Ombai Strait (Figure 5e–f). Active mixing and K_T increase as Ri_g decreases, with values of Ri_g less than 0.2 indicating an unstable water column. In the upper water column, high stratification associated with the permanent thermocline results in high Ri_g values and low K_T values. Thus, high diffusivity values over the sill in Figure 5e are significant. It could be argued that they are a benthic boundary response, but high shear in the major axes results from a beam of baroclinic tides, and not a boundary-layer effect, indicating the baroclinic tide increases the shear and K_T.

Mixing is apparent in the temperature differences over 7.5 days (Figure 5d). Generally, there is a loss of heat from the upper 200 m and a gain between ~250–

flanks in the regions of high K_T (Figure 5e) may induce most of the temperature differences with advection spreading them away from the sill.

SUMMARY
We used a 3-D, primitive equation, terrain-following coordinate model (ROMS) to simulate the M$_2$ barotropic and baroclinic tides in the Indonesian seas. Model estimates of elevation and major axes of the tidal ellipses agreed well with T/P crossover and current-meter mooring observations for the model resolution (5 km). Rms differences between the model estimates and observations were 18 cm and 13° for the elevation amplitudes and phases. Discrepancies were attributed to the coarse resolution and/or inaccuracies in bathymetry and hydrography.

Strong, baroclinic M$_2$ tides were generated along the shelf slope break and over rough topography, particularly in straits. The baroclinic tidal velocities exceeded the barotropic velocities over most of the domain, with the maximum baroclinic tidal major axes within the water column > 5 cm s^{-1} over nearly the

Of particular interest, strong baroclinic tides often coincided with important Indonesian throughflow choke points in straits where measurements were needed to quantify the flow of Pacific water that passes through the Indonesian seas into the Indian Ocean (Sprintall et al., 2004). For example, the Ombai Strait revealed the largest baroclinic tides, in excess of 50 cm/s, with mid-water column tidal velocity maximums. The Ceram Sea was also a region of interference when considering the barotropic tides alone, because the tide originating from the north (Pacific) in the Halmahera and Maluku Seas met the tide originating in the Indian Ocean, which propagated through Makassar Strait and the Banda Sea. The different propagation paths resulted in different phases and the destructive interference causes low tidal elevations. In addition, the Lombok Strait, possibly the location of a planned Directed Research

Initiative by the Office of Naval Research (Characterization and Modeling of Archipelago Strait Dynamics), was one of the most baroclinic regions revealed by the model, yet appeared to have a fairly smooth barotropic tide regime with little contrast in phase north of the strait versus south of the strait in the Indian Ocean. Because internal tides induce vertical mixing due to the increase in shear, all these "choke point" straits also have a highly depth-dependent mixing variability that will contribute to the considerable modification of the Indonesian seas thermohaline characteristics before they are exported to the Indian Ocean.

These coarse-resolution results are useful as a qualitative indicator for planning observational or higher-resolution modeling studies. For more accurate quantitative estimates, higher horizontal and vertical resolutions are required. Improved performance can also be obtained through more accurate bathymetry and hydrography. Only one semidiurnal constituent was used for this study, although multiple constituents interact. The tidal fields are affected not only through integration of the constituents, but also through fortnightly beating effects and harmonic transfer of energy between constituents. Observations have shown that fortnightly beating is associated with very strong baroclinic tides and high mixing (Hatayama, 2004; Susanto et al., 2000; Ffield and Gordon, 1996). Another limitation of the ROMS model is its inability to simulate the lee waves generated by the interactions of barotropic tides with topography. This limitation is inherent in the hydrostatic assumption and simulation of the lee waves would require switching to a non-hydrostatic model. Both multiple-constituent simulations to evaluate the transfer of energy between frequencies and finer-resolution simulations are presently in progress, but not non-hydrostatic simulations by these authors. In the future, we plan to focus on high-resolution simulations of the strait regions and to investigate the effects of the seasonal changes in the hydrography on the baroclinic tidal fields.

ACKNOWLEDGEMENTS

REFERENCES

Cresswell, G.R., and J.L. Luick. 2001. A note on current measurement in the Halmahera Sea. *Journal of Geophysical Research* 106:13,945-13,951.

Egbert, G.D., and S. Erofeeva. 2002. Efficient inverse modeling of barotropic ocean tides. *Journal of Atmospheric and Oceanic Technology* 19:22,475-22,502.

Ffield, A., and A.L. Gordon. 1996. Tidal mixing signatures in the Indonesian seas. *Journal of Physical Oceanography* 26:1,924-1,935.

Garrett, C. 2003. Internal tides and ocean mixing. *Science* 301:1,858-1,859.

Hatayama, T. 2004. Transformation of the Indonesian throughflow water by vertical mixing and its relation to tidally generated internal waves. *Journal of Oceanography* 60:569-585.

Hatayama, T., T. Awaji, and K. Akitomo. 1996. Tidal currents in the Indonesian seas and their effect on transport and mixing. *Journal of Geophysical Research* 101:12,353-12,373.

Holloway, P.E. 2001. A regional model of the semidiurnal internal tide on the Australian North West Shelf. *Journal of Geophysical Research* 106:189,625-19,638.

Luick, J.L., and G.R. Cresswell. 2001. Current measurements in the Maluku Sea. *Journal of Geophysical Research* 106:13,953-13,958.

Martinsen, E.A., and H. Engedahl. 1987. Implementation and testing of a lateral boundary scheme as an open boundary condition in a barotropic ocean model. *Coastal Engineering* 11:603-627.

Mazzega, P., and M. Bergé. 1994. Ocean tides in the Asian semi-enclosed seas from *TOPEX/POSEIDON*. *Journal of Geophysical Research* 99:24,867–24,881.

Molcard, R., M. Fieux, and F. Syamsudin. 2001. The throughflow within Ombai Strait. *Deep-Sea Research* 48:1,237–1,253.

Munk, W., and C. Wunsch. 1998. The moon and mixing: Abyssal recipes II. *Deep-Sea Research* 45:1,977–2,010.

Pawlowicz, R., R. Beardsley, and S. Lentz. 2002. Classical tidal harmonic analysis with error analysis in MATLAB using T_Tide. *Computers and Geoscience* 28:929–937.

Robertson, R., A. Beckmann, and H. Hellmer. 2003. M_2 tidal dynamics in the Ross Sea. *Antarctic Science* 15:41–46.

Robertson, R. 2005a. Barotropic and Baroclinic tides in the Ross Sea. *Antarctic Science* 17:107–120.

Robertson, R. 2005b. Barotropic and baroclinic tides in the Weddell Sea. *Antarctic Science*.

Robertson, R. Submitted. Modeling internal tides: Resolution, parameterization, and performance. *Ocean Dynamics*.

Schiller, A. 2004. Effects of explicit tidal forcing in an OGCM on the water-mass structure and circulation in the Indonesian throughflow region. *Ocean Modelling* 6:31–49.

Simmons, H.L., R.W. Hallberg, and B.K. Arbic. 2004. Internal wave generation in a global baroclinic tide model. *Deep-Sea Research II* 51:3,043–3,068.

Smith, W.H.F., and D.T. Sandwell. 1997. Global seafloor topography from satellite altimetry and ship depth soundings. *Science* 277:1,956–1,962.

Sprintall, J., S. Wijffels, A.L. Gordon, A. Ffield, R. Molcard, R.D. Susanto, I. Soesilo, J. Sopaheluwakan, Y. Surachman, and H.M. van Aken. 2004. INSTANT: A new international array to measure the Indonesian throughflow. *Eos Transactions of the American Geophysical Union* 85:369–376.

Susanto, R.D., and A.L. Gordon. 2005. Velocity and transport of the Makassar Strait throughflow. *Journal of Geophysical Research* 110:C01005, doi:10./1029/2004JC002425.

Susanto, R.D., A.L. Gordon, J. Sprintall, and B. Herunadi. 2000. Intraseasonal variability and tides in Makassar Strait. *Geophysical Research Letters* 27:1,499–1,502.